Testing procedures for extracting fluctuation spectra from lipid bilayer simulations

Joseph C. Albert, Lucas T. Ray, and John F. Nagle

Articles you may be interested in

Predicting solute partitioning in lipid bilayers: Free energies and partition coefficients from molecular dynamics simulations and COSMOmic
J. Chem. Phys. **141**, 045102 (2014); 10.1063/1.4890877

Coarse-grain simulations of active molecular machines in lipid bilayers
J. Chem. Phys. **138**, 195101 (2013); 10.1063/1.4803507

Thermal fluctuations in shape, thickness, and molecular orientation in lipid bilayers
J. Chem. Phys. **135**, 244701 (2011); 10.1063/1.3660673

Simulations of edge behavior in a mixed-lipid bilayer: Fluctuation analysis
J. Chem. Phys. **126**, 045105 (2007); 10.1063/1.2430714

Coarse-grained simulations of lipid bilayers
J. Chem. Phys. **121**, 11942 (2004); 10.1063/1.1814058

Testing procedures for extracting fluctuation spectra from lipid bilayer simulations

Joseph C. Albert,[a] Lucas T. Ray, and John F. Nagle[b]
Department of Physics, Carnegie Mellon University, Pittsburgh, Pennsylvania 15213, USA

To address concerns about how to obtain the height-height spectrum from simulations of biomembranes, we emulated the fluctuations in real space using exact input spectra. Two different methods that have given different results in the literature were then used to extract spectra from the emulated fluctuations that were then compared to the exact input spectra. A real space method shows systematic, but small deviations attributed to splines introducing an artifactual filter. A direct Fourier method obtains accurate results when the in-plane placement of the emulated particles is uncorrelated with the out-of-plane undulations, but systematic underestimates occur when the particle placement is more realistically correlated with the undulations. Although quantitative corrections cannot be estimated from our one-dimensional model, the results are qualitatively consistent with the direct Fourier method underestimating the $1/q^2$ spectral dependence that is characteristic of a tilt degree of freedom in simulations. © *2014 AIP Publishing LLC*. [http://dx.doi.org/10.1063/1.4892422]

I. INTRODUCTION

Biomembranes are two-dimensional structures that undergo thermal fluctuations. Defining the unperturbed membrane to lie in the xy plane, the out-of-plane, transverse, small amplitude, undulational fluctuations are described by $u(x, y)$, the displacements in the z direction. These fluctuations have biological consequences[1,2] and they are used to obtain quantitative structure from experimental x-ray scattering.[3] Simulations of biomembranes in equilibrium are an important tool for validating the continuum theories which provide predictions of experimental Fourier spectra.[4–6]

Brandt *et al.*[7] performed large scale molecular dynamics simulations from which the average undulational Fourier spectrum $S_u(q) \sim \langle |u(q)|^2 \rangle$ was obtained employing a method[8–11] called the Direct Fourier (DF) method that differs from the alternative Real Space (RS) method that has been somewhat more commonly used for lipid bilayer simulations.[4,5,12,13] The DF method obtained a Fourier spectrum $S_u^{DF}(q)$ that conformed to the classical tensionless undulation spectrum[14,15] for small q,

$$S_u(q) \sim 1/q^4. \qquad (1)$$

For larger q, $S_u^{DF}(q)$ included an apparently additive term equal to a suitably normalized spectrum $S_\rho(q)$ obtained from in-plane, longitudinal, fluctuations $\rho(x, y)$ of the lipid molecules. Therefore, it was suggested that subtraction of S_ρ from $S_u^{DF}(q)$ gave the true undulation spectrum $S_u^{exact}(q)$. The major conclusion from this procedure was that there was no crossover from the tensionless $1/q^4$ undulation spectrum to the $1/q^2$ regime that is found using the RS method. A $1/q^2$ regime had been predicted by earlier theories of molecular

protrusion[4,5,16] and is now being predicted by theories of molecular tilting.[12,13,17] However, there is no proof of simple additivity,

$$S_u^{DF}(q) = S_u^{exact}(q) + S_\rho(q), \qquad (2)$$

of the transverse and longitudinal fluctuations in the DF spectrum, so a $1/q^2$ term could have been suppressed by the subtraction. The DF method has been criticized for not agreeing with RS results and with tilt theories.[13,17] This is an issue that is difficult to resolve with existing molecular dynamics simulations because limitations on the size and time scales constrain the small end of the q range, thereby making it difficult to disentangle terms with different power law behavior. This compromises the ultimate goal of determining values of the bending modulus K_c and the tilt modulus K_θ from the undulation spectra $S_u(q)$.

This paper addresses this issue by devising emulated data that input an exactly known spectrum $S_u^{exact}(q)$ and then analyzing these data with the DF method to test whether subtraction of $S_\rho(q)$ from $S_u^{DF}(q)$ returns the known $S_u^{exact}(q)$ input. In this paper, the system is simplified to a one-dimensional analogue that we construct to have the same q dependence as the two-dimensional case; Appendix A provides theoretical background for this simplification. Our numerical results show that, when lateral (x-y) and undulation (z) fluctuations are completely uncorrelated, the DF method effectively reproduces S_u^{exact}. However, upon inclusion of a simple and necessary geometric correlation, the DF method, while continuing to give accurate results for wide ranges of the parameters, generally underestimates the undulation spectrum in the q range where a $1/q^2$ term would be observable. Interestingly, the RS method also suppresses the spectrum, but only for larger q compared to the DF method, so it is generally freer from artifacts that affect the interpretation of the $S_u(q)$ spectrum.

---
[a]jcalbert@alumni.cmu.edu
[b]Author to whom correspondence should be addressed. Electronic mail: nagle@cmu.edu
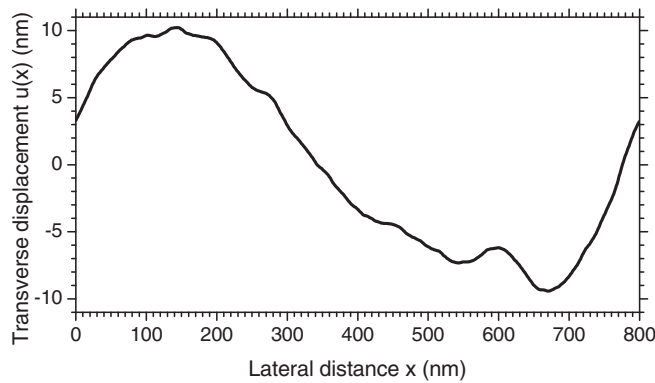
141, 064114-1

FIG. 1. Typical $u(x)$ for one set of random ϕ_m, $K_c = 20\,kT$, $\langle u \rangle = 0$, $\langle u^2 \rangle^{1/2} = 6.7$ nm.

II. TRANSVERSE FLUCTUATIONS

We begin with a 1-dimensional continuum model of length L with periodic boundary conditions. The mth harmonic is thus related to its wavenumber q_m and wavelength λ_m by

$$q_m = 2\pi/\lambda_m = \frac{2\pi m}{L}. \tag{3}$$

From Eq. (1) the amplitudes of these normal modes are postulated to be

$$u(q_m) = \frac{b' e^{i\phi_m}}{q_m^2}, \tag{4}$$

where b' is a numerical constant to be determined shortly and ϕ_m is a random phase. Real space undulations $u(x)$ are then obtained using

$$u(x) = \sum_m u(q_m) e^{iq_m x} = \sum_m \frac{b'}{q_m^2} e^{i(q_m x + \phi_m)}, \tag{5}$$

where the ϕ_m are generated as random numbers over a uniform distribution in the range $[0, 2\pi]$. For real $u(x)$, the sums include negative m with $\phi_{-m} = -\phi_m$. Figure 1 shows $u(x)$ for one set of random ϕ_m. To emulate thermal averages, many random sets are generated, each corresponding to an MD snapshot. Note that, while the phases are random, b' is an exact number, so $|u(q)|^2$ is precisely known and is the same for each emulated microstate. This eliminates an uncertainty inherent in MD simulations and accounts for our use of the word emulations instead of simulations.

III. DISCRETIZATION

As lipid membranes are comprised of discrete molecules, an MD simulation only gives $u(x_n)$ at discrete values of x_n, $n = 1, \ldots, N$. Crucially, the lateral coordinates x_n may not be evenly spaced, so the surface $u(x)$ cannot be described by a simple discrete Fourier transform. The RS method addresses this problem by interpolating $u(x_n)$ onto a uniform x grid which is then Fourier analyzed to obtain $u(q_m)$. The DF method calculates the $u(q_m)$ directly from the simulated $u(x_n)$

using

$$u(q_m) = \frac{1}{N} \sum_{n=1}^{N} u(x_n) e^{-iq_m x_n}, \tag{6}$$

where the 1/N normalization factor is required for consistency with Eq. (5).

We now discuss and quantify the b' parameter in Eq. (4). Appendix A shows that the thermally averaged height-height spectrum is given by

$$\langle |u(q_m)|^2 \rangle = \frac{kT}{K_c N^2 a^2 q_m^4}, \tag{7}$$

where kT is the thermal energy, K_c is the bending modulus, and $a = L/N$ is the mean distance between points. Following Brandt et al.,[7] it is convenient to compare different values of N on the same plot by defining the normalized undulation spectrum

$$S_u(q_m) = N^2 \langle |u(q_m)|^2 \rangle. \tag{8}$$

This normalization will be used both for the DF spectrum $S_u^{DF}(q_m)$ and for the exact input spectrum $S_u^{exact}(q_m)$. With this normalization,

$$S_u^{exact}(q_m) = b^2/q_m^4, \tag{9}$$

where

$$b^2 = \frac{kT}{K_c a^2}, \tag{10}$$

and the b' in Eqs. (4) and (5) equals b/N. Appropriate biophysical choices for the parameters are $K_c/kT = 20$ and $a = 0.8$ nm, giving $b = 0.28$ nm^{-1}. This choice places $S_u(q)$ on a similar scale as Fig. 3 in Brandt et al.[7]

Although the x_n are not located on a uniform grid in a simulation of a fluid phase bilayer, it is illuminating to consider a kind of "crystalline" case for which the x_n are chosen to be precisely at $x_n = (n - 1)a$, for n from 1 to N. As is well known in solid state physics, Fourier spectra of lattices consist of Brillouin zones that repeat in q space where the boundary of the first Brillouin zone is $\pi/a = q_B > q_m > -q_B$. Unlike the continuum case where the value of q is unlimited, for the discrete system, any q outside the first Brillouin zone is equivalent to a q in the first Brillouin zone that differs by integer multiples of $2\pi/a$. Figure 2 shows the result of applying Eq. (6) to Eq. (5) where the independent q modes were restricted to the first Brillouin zone with amplitudes given by Eq. (4). The inset emphasizes the repeating Brillouin zones that are replicated by Eq. (6). The main figure emphasizes that Eq. (6) reproduces the input $|u(q_m)|^2$ exactly. One also sees that our real space method essentially applies a filter that underestimates the true spectrum near q_B. We used a monotone piecewise cubic interpolation[18] to obtain a smooth $u(x)$ on a grid, where the result did not depend significantly on the grid size when it was smaller than about one third of the lattice spacing.

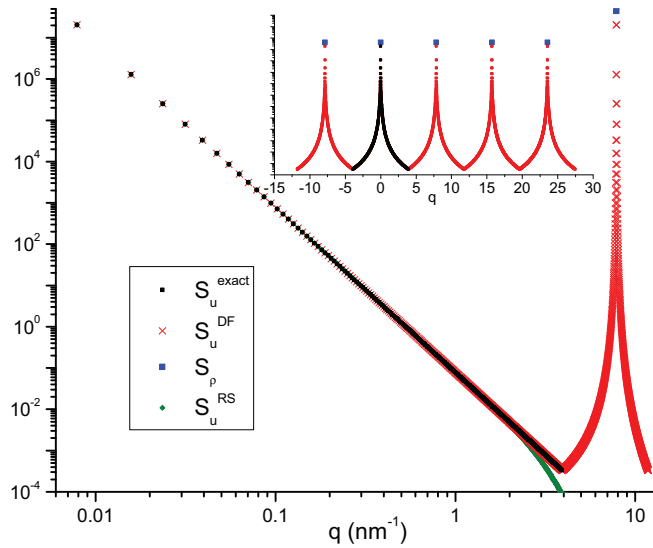The lateral density consists of delta function particles located at positions x_n. The Fourier components of the

FIG. 2. A "crystalline" case with particles placed laterally on a uniform grid and with the input parameters in Figure 1. The exact input q_m^{-4} undulation modes are shown as black squares and the direct Fourier method produces the red ×'s that are periodic in successive Brillouin zones as emphasized in the inset. The in-plane structure factor $S_\rho(q)$ is a sum of delta functions located at $2\pi h/a$ for integer h, indicated by the large blue squares. Also shown with green diamonds is a real space result S_u^{RS} obtained using a cubic spline interpolation.

longitudinal lateral density fluctuations are then

$$\rho(q_m) = \frac{1}{N} \sum_n^N e^{-iq_m x_n}, \qquad (11)$$

and the thermal average of $\langle |\rho(q_m)|^2 \rangle$ is the usual longitudinal structure factor. Following Brandt *et al.*,[7] the corresponding normalized in-plane structure factor is defined to be

$$S_\rho(q_m) = N^2 \langle u^2 \rangle \langle |\rho(q_m)|^2 \rangle, \qquad (12)$$

where $\langle u^2 \rangle$ is the thermal average of the average over lattice sites of the mean square transverse displacements in real space,

$$\langle u^2 \rangle \equiv \left\langle \frac{1}{N} \sum_{n=1}^N |u(x_n)|^2 \right\rangle, \qquad (13)$$

which corresponds to the factor introduced by Brandt *et al.* and which gives S_ρ the same physical dimensions and high-q limit as S_u.[7]

For the crystalline case, $S_\rho(q_m)$ is a delta function comb, namely, zero except when $q = 2\pi h/a$ for integer h. Therefore, subtraction does not affect the exact agreement of the DF result with the exact spectrum except at these peak values. These values of q correspond to $q = 0$ in the first Brillouin zone for which $u(q = 0)$ is undefined in Eq. (4). Physically, the $q = 0$ mode describes uniform translation in z, which is excluded in simulations by the placement of $z = 0$ to correspond to the center of mass in the z direction for each snapshot. The question now becomes whether the DF method is a good approximation for fluid phase simulations and over what range of q it may apply. For that, we turn in Sec. IV to adding lateral displacements to the uniformly spaced particle positions.

We end this section by noting that there is no advantage to extending the input values of $|u(q_m)|^2$ for q_m outside the first Brillouin zone; when many sets of ϕ_m phases are averaged, their amplitudes are simply added to the values in the first Brillouin zone; these additions only subject $S_u^{DF}(q)$ to negligible random noise near the zone boundaries.

IV. LATERAL FLUCTUATIONS

The main consideration for adding lateral fluctuations is how to choose the x_n values. We have tried three different models. (i) Independent random displacement δ_n of each x_n from its gridded value na neglects any correlation caused by interactions between nearest neighbors. It can be shown that this model gives a q^2 dependence to the $S_\rho(q_m)$ spectra. As this is unlike the MD simulations and as the model does not respect interactions between neighboring particles, we do not show any results for this artificial model. (ii) Assuming harmonic interactions between neighbors spaced a apart, the usual phonon spectrum for discrete particles has a spectrum that depends on q as $[\sin(qa/2)]^{-2}$. The appropriate emulation input is

$$\delta_n \equiv x_n - na = \sqrt{\frac{kT}{K_{lat}N}} \sum_{m=1}^{N/2} \frac{\cos(q_m na + \theta_m)}{\sin(q_m a/2)}, \qquad (14)$$

where the θ_m are random phases and K_{lat} is the harmonic spring constant. Appendix B raises the interesting, but not crucial, issue of discrete versus continuum input spectra. (iii) We have mainly generated the x_n values using a stochastic method, reminiscent of the so-called paracrystalline model,[19,20] which, unlike model (i) but like model (ii), correlates the displacements between neighboring particles. Particle 1 is placed at $x_1 = 0$ and then subsequent positions, $n = 2, \ldots, N + 1$, are iteratively computed using

$$\tilde{x}_n = \tilde{x}_{n-1} + a + \delta_n, \qquad (15)$$

where δ_n is a random number generated over a gaussian distribution centered at 0 that has root mean square value σ_{lat}. This creates a dependence between nearest neighbor separations, not unlike real neighboring atoms. However, this does not guarantee periodic boundary conditions because $\tilde{x}_{N+1}$ is only accidentally located at $(N + 1)a$, so each $\tilde{x}_n$ is rescaled by the factor

$$f = \frac{Na}{\tilde{x}_{N+1} - \tilde{x}_1}. \qquad (16)$$

For any of the three methods of generating the lateral fluctuations, one set of δ_n generated one "snapshot" of the lateral fluctuations of discrete particles. Many random sets of δ_n were similarly generated while also generating sets of random ϕ_m for the transverse fluctuations and averages were then taken over a number W of these "snapshots." Once the x_n were chosen, we considered two options for choosing the value of $u(x_n)$. Option 1 uses Eq. (5); this keeps the particles on the postulated, continuum $u(x)$ surface. Option 2 sets $u(x_n)$ equal to its value at $x = na$ calculated on the grid; this takes the particle off the original $u(x)$ surface, thereby involving protrusions, although these protrusions are highly correlated
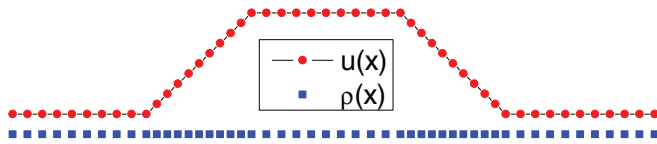
FIG. 3. Exaggerated schematic emphasizing that non-zero derivatives in $u(x)$ lead to larger lateral density $\rho(x)$.

with the lateral fluctuations. We found that the differences in $S_u^{DF}(q)$ using these two options are negligible for physically realistic values of K_c because there is little difference in the $u(x_n)$ and the $u(na)$ values; subsequent results are given only for option (1).

There is, however, an important oversight in the above procedures for generating the x_n. A reasonable expectation is that the average distance between neighbors will be the same along the $u(x)$ curve. As shown for the exaggerated example in Fig. 3, this leads to a higher density $\rho(x)$ for larger slopes in $u(x)$. This introduces correlations between $u(x)$ and $\rho(x)$ not represented in previous methods of generating sets of $\{x_n\}$ and $\{u(x_n)\}$, but which must exist in a physical system. This effect was achieved in our emulations by first generating a surface $u(x)$ as described in (5) and a set of lateral positions $\{x_n\}$ by one of the methods detailed above. New lateral positions $\{\hat{x}_n\}$ were then calculated iteratively using

$$\int_{\hat{x}_n}^{\hat{x}_{n+a}} \alpha(x)dx = (x_{n+1} - x_n)\frac{L'}{L}, \tag{17}$$

where $\alpha(x) = \sqrt{1 + (du/dx)^2}$ and the total length is

$$L' = \int_0^L \alpha(x)dx. \tag{18}$$

This has the effect that fractional position of the particle $\hat{x}_n$ along the length of the curve $u(x)$ with total length L' is equal to the fractional position of x_n along the flat line of length L. Note that the periodic boundary condition $\hat{x}_{N+1} = L$ follows by summing Eq. (17) over n because $x_{N+1} = L$ from Eq. (16), so this construction enforces periodic boundary conditions and it ensures that nearest-neighbor spacings are calculated tangent to the curve $u(x)$.

The input descriptors for each emulation are the number of particles N (we only show $N = 1000$), the average spacing between particles a (we use $a = 0.8$ nm, corresponding to an area/lipid of 0.64 nm^2 (Ref. 21)), the bending modulus K_c, the average root mean square nearest neighbor lateral fluctuation σ_{lat}, and the number W (always 10^4) of our uncorrelated snapshots. (If we suppose that $10\,ps$ snapshots are reasonably uncorrelated, $W = 10^4$ would be obtained from a 100 ns simulation.) Some output descriptors are the root mean square transverse fluctuation $\sigma_{trans} = \langle u^2\rangle^{1/2}$ (from Eq. (13), noting that $\hat{x}_n$ are used when correlations are included), and the root mean square longitudinal deviation, $\langle\langle(x_n - na)^2\rangle^{1/2}\rangle$, which is typically about 15 times greater than σ_{lat} for $N = 1000$.

V. RESULTS

Figure 4 shows the results of adding lateral fluctuations to a system that has a spectrum consisting of a sum of $1/q^4$ and
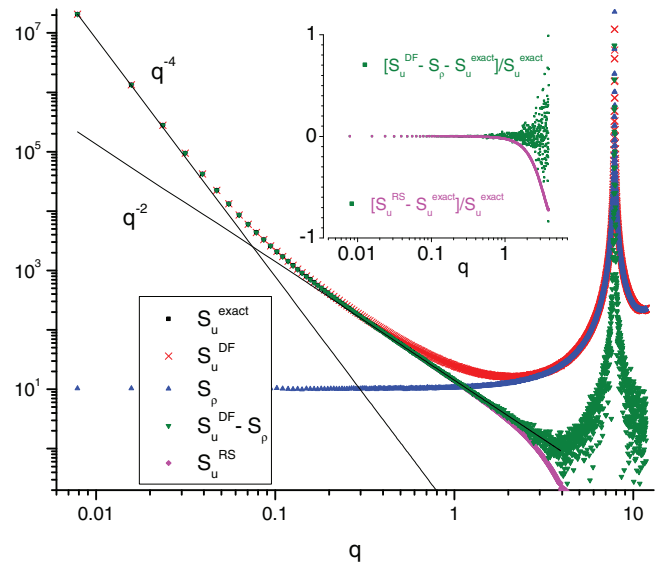

FIG. 4. Results for paracrystalline lateral fluctuations and particle placement uncorrelated with undulations, averaged over $W = 10^4$ snapshots, with $\sigma_{lat} = 0.012$ nm, to a 1-d system of $N = 1000$ particles with average separation $a = 0.8$ nm and with $K_c/kT = 20$, $K_\theta = 0.11\,kT/\text{nm}^2 \sim 0.46\,mN/m$, and $\sigma_{trans} = 6.7$ nm. The inset shows the relative errors of the DF and the RS methods normalized to S_u^{exact}. The exact input adds the q^{-2} and the q^{-4} terms shown by the solid lines.

$1/q^2$ terms. With increasing q, the exact input values of $S_u(q)$ decrease and become as small as $S_\rho(q)$ at a crossover value $q_c \approx 1$ nm^{-1} near the center of a crossover region ($0.7 < q < 2$ nm^{-1}) for S_u^{DF}; after tracking S_u^{exact} for smaller q, S_u^{DF} tracks S_ρ for larger q. The choice of $N = 1000$ was made to extend the small q region by a decade compared to currently feasible atomic level or coarse-grained simulations. The choice of σ_{lat} in Figure 4 was made so that the crossover region occurs at similar values of q_c as the simulations of Brandt et al.[7] However, the factor $\langle u^2\rangle$ in S_ρ scales as N^2 as shown in Appendix C. Therefore, in order to obtain the same q_c, it is necessary that σ_{lat} in Eq. (12) be small. This means that the nearest neighbor peak in S_ρ at $q = 2\pi/a$ is much sharper than seen by Brandt et al. We also obtained a broader peak with the same q_c by reducing N and increasing σ_{lat}.

In the main panel of Fig. 4 the differences $S_u^{DF} - S_\rho$ become noisy as q increases; as expected, this noise level scales as $1/\sqrt{W}$. Furthermore, $S_u^{DF} - S_\rho$ appears to deviate strongly from S_u^{exact}, but the logarithmic plot is very misleading in this regard because it does not show negative deviations and it spreads out the distribution for small deviations. The inset shows that the deviations ($S_u^{DF} - S_\rho - S_u^{exact}$) generally average to S_u^{exact}. However, in the inset we have chosen to divide these differences by S_u^{exact} because that is the quantity one wishes to extract, and that emphasizes that the statistical deviations using the DF method become rather too large for suitable averaging as q exceeds 2 nm^{-1} when S_u^{exact} becomes very small. The RS result, by comparison, remains smooth but exhibits systematic deviations for large q as shown in the main panel of the figure. Emulations with particle placement uncorrelated with undulations have been obtained for many different values of K_c, different size N, with and without a
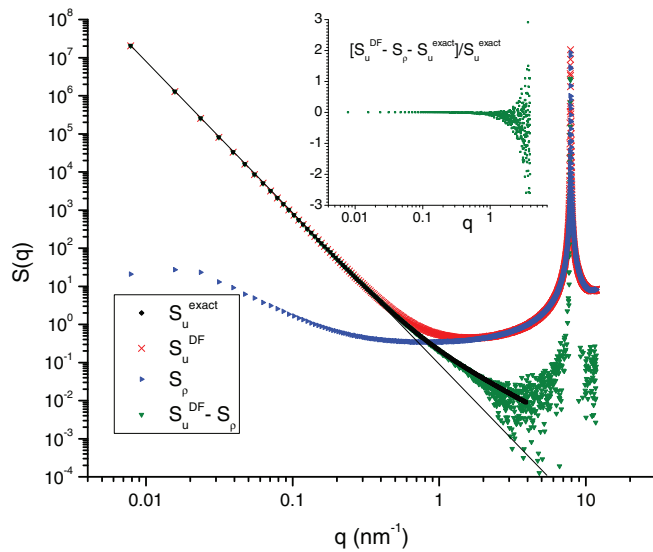
FIG. 5. Results for particle placement correlated with undulations and paracrystalline lateral fluctuations, averaged over $W = 10^4$ snapshots, with $\sigma_{lat} = 0.002$ nm, to a 1-d system of $N = 1000$ particles with average projected separation $a = 0.8$ nm and with $K_c/kT = 20$, $K_\theta = 12\,kT/nm^2 \sim 50\,mN/m$ and $\sigma_{trans} = 6.7$ nm. The inset shows the differences between $S_u^{DF} - S_\rho$ and the input values S_u^{exact} normalized to S_u^{exact}. The thin solid line shows the q^{-4} part of the exact input.

FIG. 6. Results for with correlated particle placement with $K_c/kT = 5$ and $K_\theta = 3\,kT/nm^2 \sim 13\,mN/m$ that gives $\sigma_{trans} = 13.3$ nm. Other input parameters are the same as in Fig. 5.

q^{-2} tilt term and with different amounts of lateral fluctuations σ_{lat}. The DF extracted spectrum does not show systematic deviations from the exact input.

Fig. 5 shows that correlating the particle placement with the undulations has two effects. The first is in S_ρ for $q < 1$ nm^{-1}. As shown in Fig. 3, projecting equally spaced points on the undulating curve leads to additional in-plane inhomogeneity and this accounts for a larger S_ρ, increasingly so for the small q modes that have larger S_u amplitudes. The second effect is that the DF subtraction now gives slightly smaller values than the exact input for $q > 1$ nm^{-1}, as best seen in the inset to Fig. 5. As this is in the direction of underestimating a q^{-2} term, we explored this effect further for other values of the system parameters. This underestimation became quite dramatic for smaller K_c/kT as shown in Fig. 6. Instead of following the input spectrum that has a q^{-2} tilt contribution, the DF spectrum follows the q^{-4} line up to $q = 1$ nm^{-1} and then plunges to negative values as emphasized by the inset to Fig. 6. In contrast, the RS method tracks the exact spectrum to larger q, roughly the same as in Fig. 4.

This underestimation is qualitatively similar to what is shown in Fig. 4(a) in Brandt et al.[7] There it was suggested that the negative deviations that appeared for larger q might have been due to calculating S_ρ in the projected (x, y) plane. The suggested unperformed alternative was to calculate S_ρ on the curve, which we will call S_ρ^*. Calculating S_ρ^* is essentially the same as calculating S_ρ with no correlations of particle placement with undulations; although there should be a small shift in the q values because the average distance between points exceeds a, the near constancy of the uncorrelated S_ρ should impart little difference compared to S_ρ^*. Unfortunately, and somewhat surprisingly, Fig. 7 shows that this
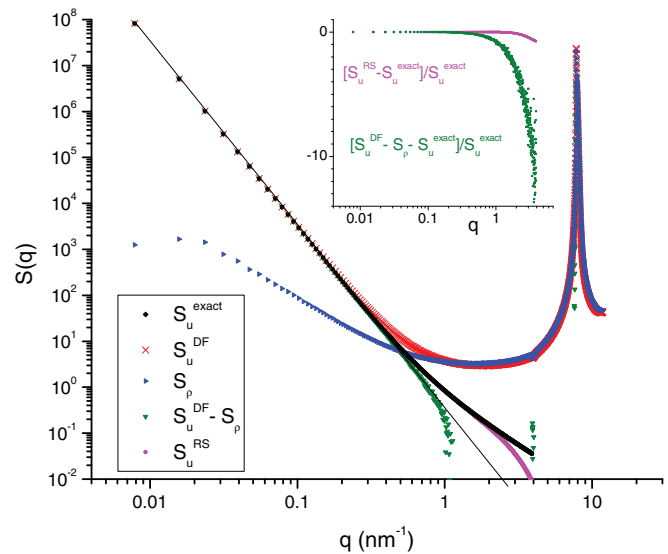
refinement of subtracting S_ρ^* from the correlated S_u^{DF} gives unacceptably large systematic positive deviations from the exact input values.

VI. DISCUSSION

Lipid bilayers have a non-zero thickness and there are distributions of different atoms along the bilayer normal. The phosphates are the favorite for describing the upper and lower membrane surfaces in simulations. The terminal methyls on the hydrocarbon chains are best for describing the center of the membrane. Large differences in $S_u^{DF}(q)$ result from this choice as seen in Fig. 2(a) in Braun et al.[22] Both choices gave the usual q^{-4} behavior in $S_u^{DF}(q)$ for small q. But for q in the
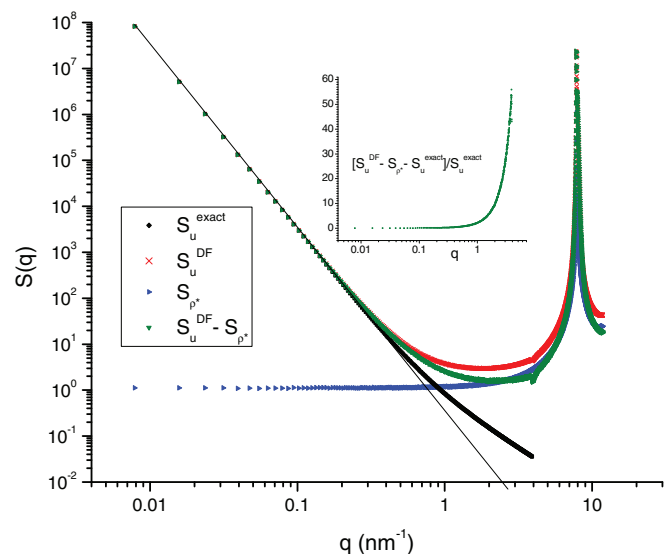

FIG. 7. Same parameters as in Fig. 6 except that the in-plane spectrum is S_ρ^* calculated along the undulating curves instead of projected onto the x axis.

range $1 - 3$ nm^{-1}, using the phosphate groups gave a strongly increasing $S_u^{DF}(q)$, whereas using the terminal methyl groups gave a nearly constant $S_u^{DF}(q)$. The latter behavior is similar to our emulations here, which is not surprising as our model has a single surface, similar to the terminal methyl surface in MD simulations. While it could have been of interest to study a model that has two surfaces emulating the phosphate groups in MD bilayer simulations, this paper has focussed on the reliability of methods for extracting the true spectra for which a single surface suffices.

We obtained many results, such as Fig. 4, for which the DF subtraction method reproduced the exact input to high accuracy when the particles were distributed with average equal spacing on the projected x axis. However, that procedure does not correlate the particle spacing with the undulations. In the uncorrelated case, Eq. (2) indeed follows as we show in Appendix D. However, as it is more realistic to distribute the particle positions on the undulating curve with equal average spacing as indicated in Fig. 3, we performed emulations with such correlations. For the typical value $K_c/kT = 20$ the DF subtraction also was rather accurate, but small systematic deviations occurred as shown in Fig. 5. Fig. 6 shows that these deviations became quite large for $K_c/kT = 5$, indicating that the DF subtraction method is incapable of dealing quantitatively with correlations between undulations and density fluctuations, even when the alternative subtraction in Fig. 7 was tried. The underestimation of the DF method occurs in a crucial q range of the spectrum that is required to extract the effect of tilt. The underestimated DF spectrum in Fig. 6 is similar to a simulated DF spectrum, from which it was concluded that tilt has no effect.[7] Although that simulation had $K_c/kT = 19$ and our emulations at $K_c/kT = 20$ do not show a similarly large effect, we do not suggest that estimates of accuracy from one-dimensional emulations should be simply transferred to two-dimensional simulations. The more significant finding in this paper is that the DF method can lead to significant underestimation of the effect of tilt on the spectrum.

Figures 4 and 6 also show that a RS spline method begins to deviate from the exact input as the boundary of the first Brillouin zone is approached, consistent with RS methods introducing an effective filter as noted by Brandt *et al.*[7] However, our results using the RS method indicate that it provides a good approximation to the spectrum up to values of q large enough to quantify either a pure q^{-4} spectrum or one involving a substantial q^{-2} additive term. This suggests that the RS method is less likely to lead to artifacts than the DF method.

APPENDIX A: COMPARISON TO 2 DIMENSIONS

Let us consider differences and similarities between the theory in one dimension vs two, beginning with a review of the two-dimensional case whose bending energy is

$$E = \frac{K_c}{2} \iint_0^L (\nabla^2 u(x, y))^2 dx dy. \tag{A1}$$

Straightforward Fourier transformation gives

$$E = \frac{K_c}{2} \sum_m \sum_n |u(q_m q_n)|^2 (q_m^2 + q_n^2)^2 L^2$$
$$= \frac{K_c L^2}{2} \sum_q |u(q)|^2 q^4, \tag{A2}$$

and using the equipartition theorem then gives the well-known result,

$$\langle |u(q)|^2 \rangle = \frac{kT}{K_c} \frac{1}{(Na)^2} \frac{1}{q^4}, \tag{A3}$$

where we have also used $Na = L$, where a is the linear spacing between points and N is the number of points in a linear direction with N^2 being the total number of points. The normalized spectrum is then given by $S_u(q_m)$ in Eq. (9) with b^2 given by Eq. (10).

Now let us compare the one-dimensional analogue

$$E = \frac{K_{c1}}{2} \int_0^L \left(\frac{d^2 u(x)}{d^2 x} \right)^2 dx, \tag{A4}$$

which immediately shows that K_{c1} has the units of energy times distance, unlike K_c in Eq. (A1) which has units of energy. Again Fourier transform of $u(x)$

$$E = \frac{K_{c1}}{2} \int_0^L \left(\sum_m -u(q_m) q_m^2 e^{iq_m x} \right) \left(\sum_n -\bar{u}(q_n) q_n^2 e^{-iq_n x} \right) dx \tag{A5}$$

$$= \frac{K_{c1}}{2} \sum_m \sum_n u(q_m)\bar{u}(q_n) q_m^2 q_n^2 \int_0^L e^{i(q_m - q_n)x} dx$$
$$= \frac{K_{c1} L}{2} \sum_m |u(q_m)|^2 q_m^4. \tag{A6}$$

To conform to the two-dimensional case, we now set $K_{c1} = K_c L$. Then,

$$E = \frac{K_c L^2}{2} \sum_m |u(q_m)|^2 q_m^4. \tag{A7}$$

Applying the equipartition theorem to each mode gives the same result as Eq. (A3) and the subsequent renormalization gives the same $S_u(q_m)$ in Eq. (9) with b^2 given by Eq. (10).

An alternative way to derive the one-dimensional analogue is to assign an infinitely stiff bending modulus K_{cy} to curvature in the y direction of a two-dimensional membrane while retaining a finite K_{cx} in the x direction. Then,

$$E = \frac{1}{2} \iint_0^L \left(K_{cx}^{1/2} \frac{d^2 u(x, y)}{d^2 x} + K_{cy}^{1/2} \frac{d^2 u(x, y)}{d^2 y} \right)^2 dx dy, \tag{A8}$$

and the Fourier transformation gives

$$E = \frac{1}{2} \sum_m \sum_n |u(q_m q_n)|^2 (K_{cx}^{1/2} q_m^2 + K_{cy}^{1/2} q_n^2)^2 (L)^2. \quad (A9)$$

Any mode with non-zero q_n has infinite energy and therefore zero amplitude, so the equipartition theorem directly gives

$$\langle |u(q_m)|^2 \rangle = \frac{kT}{K_{cx}} \frac{1}{(Na)^2} \frac{1}{q_m^4}, \quad (A10)$$

equivalent to Eq. (A3). These similarities support using the $d = 1$ model for our study.

APPENDIX B: COMPARISON OF DISCRETE AND CONTINUUM MODELS FOR FLUCTUATIONS

Figure 8 addresses the generation of lateral fluctuations with the paracrystalline method versus the phonon method. When Eq. (14) was used for the phonon method, the results were too close to those for the paracrystalline method to be visually distinguishable. Instead, the comparison in Figure 8 is to the continuum phonon case which replaces $\sin(qa/2)$ in Eq. (14) with the long wavelength limiting $qa/2$ behavior. Using the continuum phonon spectrum gives the artifact of a discontinuous derivative at the Brillouin zone boundary compared to the discrete phonon model and the paracrystalline model.

The comparison of discrete and continuum phonon generation raises a similar issue regarding transverse fluctuations. If one uses the discrete version for the bending energy, then

$$S_u^{exact}(q) = b^2 (a/2\sin(qa/2))^4. \quad (B1)$$

As Figure 9 shows, this leads to a q^{-2} contribution when analyzed for power law behavior. However, the coefficient of the q^{-2} contribution is only 1/6 as large as the coefficient of the q^{-4} term, so it only exhibits noticeable devia-
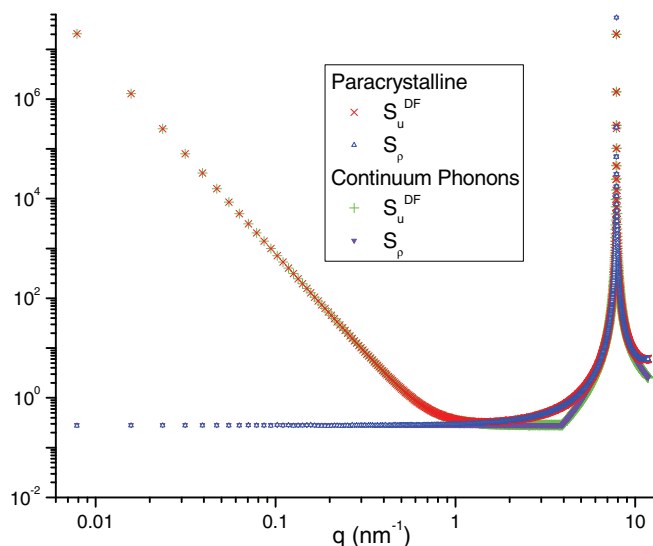

FIG. 8. Comparison of results obtained with paracrystalline generation and discrete phonon generation of lateral fluctuations are indistinguishable in this figure. The phonon result shown is for phonon generation using a continuum model. Input parameters are the same as in Figure 4 except that $\sigma_{lat} = 0.0018$ nm for the phonon case.
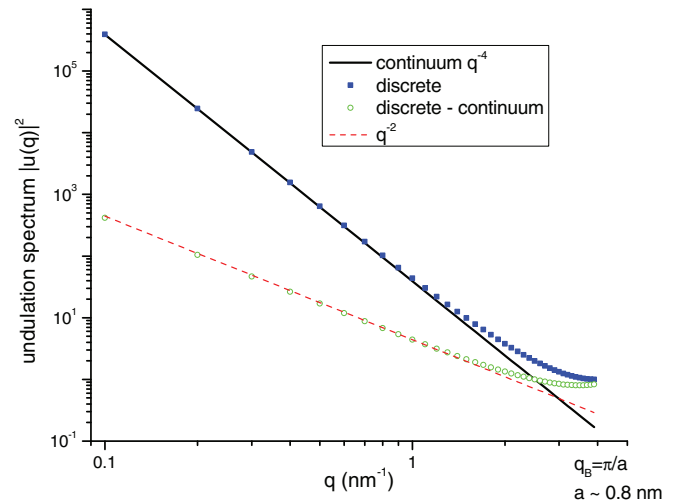

FIG. 9. Comparison of undulation spectra when a continuum model is used (solid black line) versus a discrete model (blue squares). The difference (open green circles) is well represented over the range available to simulations by a q^{-2} term (dashed red line).

tions from q^{-4} behavior when q exceeds 1 nm^{-1} as shown in Figure 9.

APPENDIX C: MEAN SQUARE DEVIATIONS IN $d = 1$ AND $d = 2$

The mean square deviation $\langle u^2 \rangle$ plays a role in comparing $S_\rho(q)$ with $S_u(q)$. It is useful to know how this quantity depends upon the size of the system, in both $d = 1$ and $d = 2$ dimensions. In one dimension, using Eq. (5) and $b' = b/N$

$$\langle u^2 \rangle \equiv \frac{1}{L} \int_0^L |u(x)|^2 dx$$

$$= \sum_m \frac{b^2}{N^2} \frac{1}{q_m^4} = \frac{2b^2 N^2 a^4}{(2\pi)^4} \sum_{m=1}^{N/2} \frac{1}{m^4} \sim N^2. \quad (C1)$$

The final sum depends only weakly upon N, going from 1 at $N = 2$ to $\zeta(4) \approx 1.0823$, so $\langle u^2 \rangle$ scales as N^2.

In two dimensions

$$\langle u^2 \rangle \equiv \frac{1}{(L)^2} \iint_0^L |u(x, y)|^2 dx dy$$

$$= \frac{4b^2 N^2 a^4}{(2\pi)^4} \sum_{n,m=1}^{N/2} \frac{1}{(n^2 + m^2)^2} \sim N^2, \quad (C2)$$

so the mean square amplitude diverges as the square of the linear size N and L for both the $d = 1$ and $d = 2$ systems.

APPENDIX D: DERIVATION OF CONDITIONS FOR VALIDITY OF THE DIRECT FOURIER METHOD

In this appendix, we first show that the direct Fourier spectrum $S_u^{DF}(q)$ is equal to the true fluctuation spectrum $u^{exact}(q)$ convolved with the lateral density structure factor $\rho(q)$ and multiplied by a constant. We further show that in relevant limits this expression reduces to the additive relation

(2) posited by Brandt *et al.* when $\rho(q)$ is uncorrelated with $u^{exact}(q)$.

S_u^{DF} is defined by

$$S_u^{DF}(q) \equiv N^2 \left\langle \left| \frac{1}{N} \sum_{n=1}^{N} u(x_n) e^{-iqx_n} \right|^2 \right\rangle. \quad \text{(D1)}$$

This can be written as an integral of the summand times N delta functions

$$S_u^{DF}(q) = N^2 \left\langle \left| \int_{x=0}^{\infty} u(x) e^{-iqx} \left(\sum_{n=1}^{N} \delta(x - x_n) \right) dx \right|^2 \right\rangle. \quad \text{(D2)}$$

By the convolution theorem, the Fourier transform of this product is the convolution of the individual transforms of $u(x)$ and the sum of delta functions, denoted $w(x)$. Consequently,

$$S_u^{DF}(q) = N^2 \left\langle \left| \int_{-\infty}^{\infty} u(q') w(q - q') dq' \right|^2 \right\rangle, \quad \text{(D3)}$$

where $w(q)$ is

$$w(q) = \int_{x=0}^{L} \frac{1}{N} \left(\sum_{n=1}^{N} \delta(x - x_n) \right) e^{-iqx} dx$$

$$= \frac{1}{N} \sum_{n=1}^{N} e^{-iqx_n} = \rho(q). \quad \text{(D4)}$$

The $\rho(q)$ in Eq. (D4) is exactly the lateral density fluctuation components in Eq. (11). Thus, the direct Fourier spectrum S_u^{DF} in Eq. (D1) is equal to the square of the convolution of the true undulation spectrum $u(q)$ with the lateral density spectrum $\rho(q)$, multiplied by a factor of N^2. The analysis so far has been identical to that done for non-equispaced time series by Ref. 23. Unfortunately, as noted in Ref. 23, deconvolving Eq. (D3) to get the u is not always feasible when working with actual, noisy data.

We next demonstrate that Eq. (D3) reduces to Eq. (2) proposed in Ref. 7, if lateral fluctuations are sufficiently small and statistically uncorrelated with undulations. Crucially, if either of these conditions is violated, the additive relation Eq. (2) will not necessarily hold.

Substituting Eq. (D4) into (D3) and using the assumption of periodic boundary conditions on $u(q)$ gives

$$S_u^{DF}(q_m) = N^2 \left\langle \left| \sum_{q_p} u(q_p) \rho(q_m - q_p) \right|^2 \right\rangle. \quad \text{(D5)}$$

Assuming the u and ρ modes are uncorrelated, then

$$S_u^{DF}(q_m) = N^2 \sum_{q_p} \langle |u(q_p)|^2 \rangle \langle |\rho(q_m - q_p)|^2 \rangle. \quad \text{(D6)}$$

Separating the terms with $\rho(0)$ factors, noting that $\rho(0) = 1$, and recalling that $|u(q)| = |u(-q)|$,

$$S_u^{DF}(q_m) = N^2 \left(\langle |u(q_m)|^2 \rangle + \sum_{q_p > 0, q_p \neq q_m} 2\langle |u(q_p)|^2 \rangle \right.$$

$$\left. \times \frac{(\langle |\rho(q_m + q_p)|^2 \rangle + \langle |\rho(q_m - q_p)|^2 \rangle)}{2} \right). \quad \text{(D7)}$$

In q regions where ρ does not have significant curvature and can be approximated as the mean of $\rho(q \pm \epsilon)$ for small ϵ, one obtains

$$S_u^{DF}(q_m) \approx N^2 \left(\langle |u(q_m)|^2 \rangle + \langle |\rho(q_m)|^2 \rangle \sum_{q_p > 0 \neq q} 2\langle |u(q_p)|^2 \rangle \right)$$

$$\approx S_u^{exact}(q_m)(1 - \langle |\rho(q_m)|^2 \rangle) + S_\rho(q_m). \quad \text{(D8)}$$

In our emulations and likely for actual simulations, $\langle |\rho(q)|^2 \rangle$ is small compared to unity, so this reduces to Eq. (2).

[1] Y. Shibata, J. J. Hu, M. M. Kozlov, and T. A. Rapoport, Annu. Rev. Cell Dev. Biol. **25**, 329 (2009).

[2] L. V. Chernomordik and M. M. Kozlov, Annu. Rev. Biochem. **72**, 175 (2003).

[3] Y. Liu and J. F. Nagle, Phys. Rev. E **69**, 040901 (2004).

[4] E. Lindahl and O. Edholm, Biophys. J. **79**, 426 (2000).

[5] R. Goetz, G. Gompper, and R. Lipowsky, Phys. Rev. Lett. **82**, 221 (1999).

[6] J. F. Nagle, M. S. Jablin, S. Tristram-Nagle, and K. Akabori, "What are the true values of the bending modulus of simple lipid bilayers?," Chem. Phys. Lipids (in press).

[7] E. G. Brandt, A. R. Braun, J. N. Sachs, J. F. Nagle, and O. Edholm, Biophys. J. **100**, 2104 (2011).

[8] W. K. den Otter and W. J. Briels, J. Chem. Phys. **118**, 4712 (2003).

[9] J. Stecki, J. Chem. Phys. **120**, 3508 (2004).

[10] J. Stecki, Adv. Chem. Phys. **144**, 157 (2010).

[11] J. Stecki, J. Chem. Phys. **137**, 116102 (2012).

[12] E. R. May, A. Narang, and D. I. Kopelevich, Phys. Rev. E **76**, 021913 (2007).

[13] M. C. Watson, E. G. Brandt, A. J. Welch, and F. L. H. Brown, Phys. Rev. Lett. **109**, 028102 (2012).

[14] W. Helfrich, Z. Naturforsch., C **28**, 693 (1973).

[15] W. Helfrich and R. M. Servuss, Il Nuovo Cimento D **3**, 137–151 (1984).

[16] G. Brannigan and F. Brown, Biophys. J. **90**, 1501 (2006).

[17] M. C. Watson, E. S. Penev, P. M. Welch, and F. L. H. Brown, J. Chem. Phys. **135**, 244701 (2011).

[18] F. N. Fritsch and R. E. Carlson, SIAM J. Numer. Anal. **17**, 238 (1980).

[19] R. Hosemann and S. N. Bagchi, *Direct Analysis of Diffraction by Matter* (North-Holland, Amsterdam, 1962).

[20] A. Guinier, *X-Ray Diffraction* (W. H. Freeman, San Francisco, 1963).

[21] J. F. Nagle and S. Tristram-Nagle, Biochim. Biophys. Acta, Rev. Biomembr. **1469**, 159 (2000).

[22] A. R. Braun, E. G. Brandt, O. Edholm, J. F. Nagle, and J. N. Sachs, Biophys. J. **100**, 2112 (2011).

[23] T. J. Deeming, Astrophys. Space Sci. **36**, 137 (1975).